APPENDIX:

ANALYTICAL METHODS

SHRIMP U-Pb dating

Samples for SHRIMP dating were selected from a representative suite of protoliths of meta-igneous rocks. Sample locations are shown in Figure 2. Zircon separation was by standard crushing, density, and magnetic sorting techniques. Sample and standard grains were imaged with cathodoluminescence (CL) prior to analysis and spots were chosen using the CL images to avoid inclusions, alteration, and mixed domains as well as to preferentially analyze higher U portions of the zircons for better analytical precision.

The mounts were cleaned in 1N HCl and gold-coated for maximum surface conductivity. The U-Th-Pb analyses were made using the SHRIMP-RG housed in Green Hall at Stanford University, California and co-owned by the US Geological Survey. The primary oxygen ion beam operated at about 4-6 nA and excavated an area of about 25–35 μm in diameter to a depth of about 1 μm. Data for each spot were collected in sets of five scans through the mass range. The reduced $^{207}Pb/^{206}Pb$ ratios were normalized to zircon standard WRP 03-68 (a diorite from central Colorado; 1707 Ma; Premo, personal communication) and MAD (4200 ppm U, Wooden, personal communication). Analyses of samples and standard were alternated for the closest control of Pb/U ratios. U, Th, and Pb concentrations are reproducible on the gem quality standard at ~10% (2σ) and include real heterogeneity in the standard. Data reduction follows the methods described by Williams (1998) and Ireland and Williams (2003) using SQUID (version 1.08) and ISOPLOT (version 3.00) software (Ludwig, 2002, 2003). Some of the resultant ablation

pits were imaged on a scanning electron microscope and compared with the CL images to verify spot size and that the intended domains were sampled.

CA-ID-TIMS U-Pb dating

Five single zircons from SM009 were dated by chemical abrasion (Mattinson, 2005), isotope dilution, thermal ionization mass spectrometry (CA-ID-TIMS). Three of the grains were also mechanically abraded. The zircons were annealed at 850 °C for 48 hours and dissolved in two steps. The first dissolution step used HF and HNO_3 in a 180 °C oven for 12 hours. The liquid was discarded, and the remaining grains were rinsed and cleaned in HCl and HNO_3. The samples were spiked with a mixed ^{205}Pb-^{233}U-^{235}U tracer (ET535), dissolved in concentrated HF and HNO_3 acids at 240 °C, and converted to chlorides in micro-dissolution capsules following the methods of Parrish et al. (1987). Pb and U were purified with HCl-H_2O ion exchange chemistry modified from Krogh (1973), and loaded onto rhenium filaments in silica gel and graphite, respectively, for thermal ionization mass spectrometry. Isotopic compositions were measured in multi-collector, static mode on a Micromass Sector 54 mass spectrometer at the University of Wyoming with ^{204}Pb in a Daly-photomultiplier collector and all other isotopes in Faraday collectors. Mass discrimination for Pb of 0.059±0.05%/amu was determined by replicate analyses of NIST SRM 981. U fractionation was determined internally during each run and ranged from -0.115 to -0.045%/amu. Pb blanks averaged 3.5 pg during the course of the study; U blanks were consistently less than 0.6 pg. Concordia coordinates, intercepts, weighted means, Concordia Ages and uncertainties were calculated using MacPBDAT and ISOPLOT programs based on Ludwig (1988, 1991, 1998, 2003). Initial Pb isotopic compositions were estimated from Stacey and Kramers (1975) model.

TEXTURAL AND CHEMICAL FEATURES OF ANALYZED ZIRCONS

Green Mountain Formation volcanic rocks

WRP 82-13: Zircons from WRP 82-13 are euhedral and oscillatory zoned (in CL images) indicating magmatic growth (Fig. A-1). No xenocrystic cores were observed. The short, stubby dipyramidal prisms and abundant fluid inclusions are typical of volcanic zircon. SHRIMP spots and resulting age data were taken from oscillatory-zoned regions of the grains. Twelve spots were analyzed from twelve grains (Table A-1). The weighted average $^{207}Pb/^{206}Pb$ date of 1781 ± 8 Ma is interpreted as the age of crystallization of the zircon, and within error, the age of the eruption and crystallization of the volcanic rock.

Sierra Madre Granite

WRP 81-24: See Premo and Van Schmus (1989) for sample description. Zircons from WRP 81-24 are euhedral to subhedral terminated prisms with aspect ratios ~3:1. CL images show oscillatory zoned cores overgrown by thin non-luminescent rims (Fig. A-2). These non-luminescent rims often include irregular luminescent stringers. We interpret the cores of the zircons to represent igneous growth reflecting crystallization of the granite magma. The non-luminescent overgrowths with the irregular luminescent stringers are interpreted as late, possibly hydrothermal growth. Only the igneous cores were analyzed for this study. No xenocrystic cores were observed. Twenty total spots were analyzed (Table A-1), with one rejected due to high common Pb and strong discordance. The remainder yielded a weighted average $^{207}Pb/^{206}Pb$ date of 1763 ± 9 Ma, interpreted as the crystallization age of the granite.

WRP 82-34: See Premo and Van Schmus (1989) for sample description. Zircons from this sample are euhedral with aspect ratios of ~2–3:1. CL images show oscillatory zoned cores occasionally overgrown by low-luminescence unzoned rims (Fig. A-3). We interpret these zircons to dominantly reflect igneous grown during crystallization of the granite slightly modified by later (hydrothermal?) overgrowths. No xenocrystic cores were observed. A total of 17 spots from the igneous cores were analyzed on the SHRIMP with three points rejected due to high common Pb and strong discordance (Table A-1). The remaining analyses yield a weighted average $^{207}Pb/^{206}Pb$ date of 1767 ± 9 Ma, interpreted as the crystallization age of the granite.

Metagabbro-granodiorite

SM073r: This is a medium-grained, partially amphibolitized and weakly deformed gabbronorite. Zircons from SM073r are anhedral and range from clear to faint purple (Fig. A-4). CL images show oscillatory zoning throughout most of the grains (Fig. A-5). Portions of the grains are modified by high luminescence regions, which crosscut and obscure original oscillatory zoning and often follow original sector zones. The outer portions of the grains have thin, discontinuous, high-luminescence rims. We interpret the bulk of the zircon to represent igneous growth, based on the typical anhedral crystal form of zircons from mafic rocks (e.g., Scoates and Chamberlain, 1995; Corfu et al., 2003) and their oscillatory zoning (e.g., Hanchar and Miller, 1993). The crosscutting high-luminescence zones probably result from metamorphic recrystallization of original igneous zircon (e.g., Vavra et al., 1996). The thin discontinuous rims of high-luminescence zircons may represent a second phase of metamorphic overgrowth, but were too small to probe with the SHRIMP.

Spots for analysis were selected to represent igneous cores and areas of recrystallized zircon. Fifteen spots were analyzed from fifteen grains (Table A-1). Two spots were rejected because of high errors and common lead. All the remaining spots were less than 5% discordant. The weighted average $^{207}Pb/^{206}Pb$ dates of the oscillatory zoned igneous zircon and recrystallized zircon domains were 1782 ± 7 Ma and 1743 ± 14 Ma, respectively.

SM357: This sample is a fine-grained leucocratic biotite granodiorite with a solid-state foliation defined by aligned biotite grains. Zircons are stubby with aspect ratios ~2:1. They are generally faint purple with Fe-oxide staining. Corroded prisms are common suggesting resorption following magmatic growth. CL images show igneous oscillatory zoning, internal evidence for resorption and possible hydrothermal alteration, and high-luminescence overgrowths (Fig. A-6). No xenocrystic cores were observed. A total of 14 spots from 14 grains were analyzed (Table A-1). Two spots were rejected because of high common Pb – one is clearly a younger rim, similar to the overgrowth shown in Figure A-6. The remaining spots are in unaltered zircon cores interpreted as igneous growth. All but one (spot 2) of the remaining analyses fall on a discordia with an upper intercept date of 1777 ± 11 Ma and a lower intercept of 928 ± 480 Ma. Inclusion of spot 2 yields a weighted average $^{207}Pb/^{206}Pb$ date of 1775 ± 8.5 Ma (MSWD 1.90) and an upper intercept date of 1778 ± 16 Ma (MSWD 2.2). Although neither the CL images nor the chemistry provide a clear reason to reject spot 2, its clear departure from the trend of the remaining points suggests it is nonetheless anomalous. Therefore, our preferred crystallization age is 1777 ± 11 Ma.

Garnet-bearing metagabbro-granite suite

SM009: This is an orthoamphibolite composed of hornblende, plagioclase, clinopyroxene, garnet, and sparse orthopyroxene with accessory biotite, apatite, and zircon. Plagioclase forms two textural and compositional types in this sample: (1) calcic plagioclase laths up to 1 cm in length, and (2) sodic, fine-grained matrix plagioclase. The plagioclase laths and orthopyroxene grains are interpreted as relict igneous minerals. The plagioclase laths are oriented suggesting magmatic flowage, whereas the matrix plagioclase is massive and equigranular suggesting metamorphic recrystallization. Other rocks within this outcrop contain K-feldspar phenocrysts mantled with plagioclase, consistent with magma mingling. We interpret SM009 as a member of this mingled suite, slightly more felsic than SM017r (below) consistent with the presence of sparse metamorphic biotite.

Zircons from this sample are euhedral, terminated prisms with aspect ratios around 5–7:1, generally clear or rust stained (Fig. A-7A). Synneusis twins are common, consistent with magmatic growth. The acicular shape of these zircons may reflect a low degree of supersaturation in a relatively dry melt (Woensdregt, 1992; Vavra, 1994) consistent with the relatively low silica content of this rock (Watson and Harrison, 1983) and/or fast growth due to rapid undercooling (Corfu et al., 2003) consistent with chilling of a mafic magma during mixing with a cooler felsic magma. CL imaging shows some oscillatory zoning and no evidence for xenocrystic cores or metamorphic rims.

Zircons from SM009 were analyzed both by SHRIMP and CA-ID-TIMS methods. The discordance of the SHRIMP analyses (5–17%) resulted in an imprecise upper intercept date of 1767 ± 22 Ma. Our preferred crystallization age for this sample (1763.1 ± 1.6 Ma) is a Concordia Age (Ludwig, 1998) calculated from the four whole-

grain CA-ID-TIMS analyses. Combining the SHRIMP and CA-ID-TIMS analyses produces a well-defined discordia (Fig A-7B). Anchoring the upper intercept at our preferred crystallization age results in a lower intercept date of 64 Ma (Model 2 fit, MSWD = 1.4), which is consistent with the Laramide uplift age of the Sierra Madre (49–79 Ma; Kelley, 2005).

SM017r: This rock is a fine-grained orthoamphibolite with relict igneous plagioclase, clinopyroxene, and sparse orthopyroxene plus accessory Fe-Ti oxides, apatite, and zircon. Garnet is common and is interpreted throughout the garnet-bearing metagabbro as metamorphic, having grown during the breakdown of orthopyroxene at upper amphibolites-facies conditions.

Zircons from this sample are small, anhedral to subhedral, and clear to faint purple with occasional iron staining (Fig. A-8). CL images of these zircons show dark cores, commonly with faint oscillatory zoning that is overgrown and/or embayed by light rims (Fig. A-9). One of the luminescent rims shows faint relicts of original oscillatory zoning. The low-luminescence cores are interpreted as original igneous zircon that was both overgrown and recrystallized during subsequent metamorphism. The presence of subhedral crystal forms suggests that zircon saturation occurred sufficiently early in the crystallization of this rock for the zircons to grow freely in the liquid, unlike those of SM073r.

We analyzed a total of 20 points from 20 grains including both cores and rims (Table A-1). Five analyses were discarded for age determinations, two because of high common Pb (spots 5 and 9), one where very high U and Th concentrations and texture in CL suggested hydrothermal alteration (spot 8), and two where imaging of the pits

revealed that the spots had spanned multiple CL domains (spots 3 and 17). Three analyses of high luminescence domains (spots 4, 13, and 18; Fig. A-9) are interpreted as resulting from metamorphic recrystallization at ~1619 Ma. This may also be the age of the thin, high luminescence rims. The remaining analyses fall into two distinct groups based on age, Th/U ratios, and Th and U concentrations (Table A-1). The older group (~1763 Ma) has Th/U ≥ 0.59 and distinctly higher U (315–1822 ppm) and Th (224–1242 ppm) concentrations. Oscillatory zoning in the CL images suggests that these spots correspond to igneous zircon. These spots are also generally more discordant, consistent with Mattinson's (2005) suggestion that lattice strain induced by higher trace element concentration leads to greater lead loss. The younger group (~1745 Ma) has Th/U ≤ 0.29 and distinctly lower U and Th concentrations. These spots are not texturally distinct in CL other than a possible blurring of original oscillatory zoning (Fig. A-9) and may reflect diffusive Pb loss without substantial recrystallization.

SM045: This is a granodioritic augen gneiss. Primary igneous minerals are quartz, microcline, plagioclase, biotite, and hornblende along with accessory apatite, allanite, and zircon. Rocks in this outcrop are slightly migmatitic (probably less than 5% melt volume) with concordant, garnet-bearing leucosomes irregularly distributed. The presence of garnet in the leucosomes suggests biotite-dehydration melting and implies upper amphibolite-facies, syndeformational metamorphism. Sample SM045 was chosen for its lack of macroscopic leucosome and accordingly petrographic analysis shows no garnet, resorbed biotite, or relict anatectic melt veins. Therefore, growth of anatectic zircon in this sample is expected to be minimal or lacking.

These zircons are slightly rounded to euhedral terminated prisms, colorless to faint purple, with aspect ratios ~3:1. In CL, the zircons have a complex morphology reflecting several events (Fig. A-10). In the best developed examples, they show an inner core (ic), commonly with oscillatory zoning (occasionally altered), surrounded by a non-luminescent band (nl), and an outer core domain with oscillatory banding that is generally diffuse or altered (rz). No xenocrystic cores were observed. The outer core is overprinted by resorption in some grains followed by a non-luminescent, rounded overgrowth (og) that is responsible for the rounded shapes of the grains. Following the detailed analysis of similar features by Pidgeon et al. (1998), we interpret the inner core, non-luminescent band, and outer core to represent original igneous zircon modified by intracrystalline diffusion, which concentrates impurities into the non-luminescent (and possibly non-zircon) band. Pidgeon et al. (1998) attributed this intracrystalline diffusion to slow cooling of the igneous body, which may also account for the textures in these samples, although a metamorphic event relating to migmatization cannot be ruled out. The resorption and overgrowth events crosscut all internal features and are inferred to record a later metamorphic event.

A total of 20 spots were analyzed from eighteen grains including domains of both cores (ic and rz) and rims (og) (Table A-1). Two spots were rejected because of high common Pb. The remaining analyses can be grouped into two distinct clusters of analyses based on their Th/U ratios. The group with the higher Th/U ratios (> 0.2) corresponds to the oscillatory zoned cores (inner and outer, ic and rz). The group with the lower Th/U ratios (≤ 0.01) corresponds to the unzoned rims, suggesting a metamorphic origin (e.g., Rubatto, 2002). The lower Th/U ratio in metamorphic rims

from these samples compared to data from igneous oscillatory-zoned domains is due to both a decrease in Th (averages 3 vs. 89 ppm) and an increase in U (averages 715 vs. 277 ppm). This is in contrast to SM017r, in which the metamorphic analyses had significantly lower U concentrations than the igneous grains. We interpret this as reflecting the difference between metamorphic recrystallization, in which both U and Th are expelled (SM017r), and new growth from a high-U fluid/melt (SM045). The lower Th concentrations in SM045 could reflect either a lack of Th in the fluid/melt or a lower crystallization temperature.

The core analyses plot on a discordia with an upper intercept of 1769 ± 10 Ma (MSWD = 0.61). This is interpreted as the crystallization age of the rock. The grains with the best-developed non-luminescent bands (spots 2 and 7) have ages that are statistically indistinguishable from the other cores, and were included in the analysis. If these grains do represent a discrete recrystallization event, however, their weighted average $^{207}Pb/^{206}Pb$ date of 1752 ± 13 Ma provides the best estimate of the timing of that event.

The remaining points all have younger spot ages and are interpreted as dating metamorphic domains based on their low Th/U ratios, lack of oscillatory zoning, rounded shapes, and truncation of the oscillatory zoned cores in CL images. The youngest three ages are nearly concordant and have a weighted average $^{207}Pb/^{206}Pb$ date of 1618 ± 9 Ma, which is our preferred age for the metamorphism. Analyses with low Th/U and intermediate ages are interpreted as spots that sampled both the more than one domain.

SM061r: This sample is a coarse-grained hornblende-biotite granitic gneiss with a strong foliation. Zircons separated from this sample are subhedral, terminated prisms,

faint purple with some iron staining. CL images show a general morphology very similar to that of SM045 consisting of an inner oscillatory zoned core (inner core, ic), a non-luminescent band (nl), an outer oscillatory zoned region (outer core, oc), overgrown by a planar banded rim with a rounded aspect (rim, og) (Fig. A-11). No xenocrystic cores were observed. The oscillatory zoning of the outer core appears to be less sharp than that of the inner core, and the outer core is less luminescent than the inner core. The non-luminescent bands are often dark in backscatter electron images suggesting that they are not composed of crystalline zircon (Fig. A-11). The outer planar banded rims commonly crosscut oscillatory zoning in the cores implying an episode of resorption prior to final growth.

A total of 28 spots were analyzed from 22 grains (Table A-1). Two were rejected for high errors and common lead. The remaining points can be split into three groups based on their morphology as revealed in the CL images. Data from the inner, relatively luminescent, oscillatory zoned cores have a mean weighted $^{207}Pb/^{206}Pb$ date of 1759 ± 8 Ma (n = 16; MSWD 1.03). Data from 6 analyses of the outer cores have a range of $^{207}Pb/^{206}Pb$ ages from 1641–1737 Ma and represent a spread of ages, not a single population. Two of the banded outer rims were sampled and yielded $^{207}Pb/^{206}Pb$ dates of 1590 ± 27 and 1601 ± 26 Ma.

Partially recrystallized inner and outer cores separated by non-luminescent bands have been observed in earlier studies (Vavra et al., 1996; Pidgeon et al., 1998). Following their interpretations, we interpret the cores of the SM061r zircons to represent the partial recrystallization of original igneous oscillatory zoned zircon during a later metamorphic event which sequestered many of the trace elements into the non-luminescent band. Th

and the Th/U ratio are correlated in our spot analyses ($r^2 = 0.5$), whereas U and Th/U are uncorrelated ($r^2 \approx 0$), suggesting that recrystallization resulted in preferential expulsion of Th, consistent with its larger ionic radius. In this interpretation, the youngest analyses in these recrystallized zones, ~1641 Ma, would represent a maximum age of recrystallization.

SM290: This is a coarse-grained hornblende-biotite granodioritic to monzogranitic augen gneiss. Abundant accessory minerals include allanite, titanite, apatite, and zircon.

Zircons are partially resorbed, terminated prisms, which are faint purple with variable Fe staining, and show clear evidence of synneusis. CL images reveal complex internal morphologies (Fig. A-12). Zircon interiors have well-developed oscillatory zoning. No xenocrystic cores were observed. In some zircon interiors there are low luminescence, preferentially altered cores surrounded by internal resorption features. None of these cores were analyzed with the SHRIMP. We tentatively interpret these cores as an early, possibly trace element-rich and therefore more readily alterable, growth phase, which preceded the crystallization of the more voluminous oscillatory zoned zircon. The oscillatory zoned portions of the cores commonly show a range of alteration. Figure A-12 shows an apparent sequence of increasing alteration from unaltered oscillatory zoning (grain #5) to convolute zoning (grain #8). Grain #8 also shows development of thick low luminescent bands associated with blurring of primary oscillatory zoning attributed to diffusive transfer of trace elements. The igneous cores are commonly partially resorbed and then overgrown by low luminescence rims (ll) followed by high luminescence rims (hl), interpreted to reflect a later metamorphic event.

Fourteen total spots were analyzed from thirteen grains. The two lowest ages represent metamorphic rims (2.2 and 4). The $^{207}Pb/^{206}Pb$ age of the youngest analysis sets a minimum age of metamorphism at 1611 ± 22 Ma (2σ). The young overgrowths had a low Th/U ratio relative to the igneous cores. This reflects both an increase in the U concentration and a dramatic decrease in Th concentration. Similar to SM045, we interpret this as due to new crystallization from a U-rich fluid/melt. The remaining points are all from oscillatory zoned cores. However, spot 8 (Table A-1, Fig. A-12) is from a strongly modified zircon and the age is distinctly lower than the rest of the points from oscillatory zoned cores. Therefore spot 8 is interpreted as having been reset by solid-state recrystallization. The remaining points have weighted average $^{207}Pb/^{206}Pb$ date of 1765 ± 7 Ma (MSWD 0.51), which is interpreted as the igneous crystallization age of the rock. Spot 8 could represent a metamorphic event (1739 ± 30 Ma at 2σ) or partial resetting during a younger, ca. 1610 Ma, event.

Syndeformational leucosome in migmatite

SM058: Zircons extracted from SM058 are generally light purple, euhedral prisms with aspect ratios ~3:1. CL images often show resorbed and recrystallized cores overgrown by oscillatory zoned igneous zircon overgrowths (Fig. A-13). These overgrowths commonly also show resorption surfaces within them suggesting fluctuation from undersaturation to oversaturation during igneous growth, a feature that has been observed in other studies of anatectic zircon growth (e.g., Vavra, 1990; Schaltegger et al., 1999). We interpret these textural features as showing possible partially resorbed detrital xenocrystic cores overgrown by anatectic igneous zircon. Due to the large size of these zircon grains relative to those of other samples on the same mount, the centers of the

zircons were generally not exposed during sample preparation. It is possible that some of these zircons contain inherited cores that were not observed in CL images.

A total of 18 spots were analyzed from 15 grains (Table A-1). One analysis (spot 10.1) had high errors and common lead and was excluded from further interpretation. Spot 5 has a distinctly lower age than the remaining analyses and the CL image shows evidence for transgressive recrystallization, so it was interpreted as a partially reset age and excluded from further calculations. The remaining analyses lie on a well-defined discordia and provide an intercept date of 1747 ± 7 Ma (MSWD 0.63), which is interpreted as the age of anatexis and deformation.

References Cited

Corfu, F., Hanchar, J.M., Hoskin, P.W.O., and Kinny, P.D., 2003, Atlas of zircon textures: Reviews in Mineralogy and Geochemistry, v. 53, p. 469–500.

Hanchar, J.M., and Miller, C.F., 1993, Zircon zonation patterns as revealed by cathodoluminescence and backscattered electron images; implications for interpretation of complex crustal histories: Chemical Geology, v. 110, p. 1–13.

Ireland, T.R., and Williams, I.S., 2003, Considerations in zircon geochronology by SIMS: Reviews in Mineralogy and Geochemistry, v. 53, p. 215-241.

Kelley, S.A., 2005, Low-temperature cooling histories of the Cheyenne belt and Laramie Peak shear zone, Wyoming, and the Soda Creek-Fish Creek shear zone, Colorado, *in* Karlstrom, K.E., and Keller, G.R., eds., The Rocky Mountain region–An evolving lithosphere: Tectonics, geochemistry, and geophysics: American Geophysical Union Monograph 154, p. 55–70.

Krogh, T.E., 1973, A low-contamination method for hydrothermal decomposition of zircon and extraction of U and Pb for isotopic age determinations: Geochimica et Cosmochimica Acta, v. 37, p. 485-494.

Ludwig, K.R., 1988, PBDAT for MS-DOS, a computer program for IBM-PC compatibles for processing raw Pb-U-Th isotope data, version 1.24: U.S. Geological Survey, Open-File Report 88-542, 32 p.

Ludwig, K.R., 1991, ISOPLOT for MS-DOS, a plotting and regression program for radiogenic-isotope data, for IBM-PC compatible computers, version 2.75
U.S. Geological Survey, Open-File Report 91-445, 45 p.

Ludwig, K.R., 1998, On the treatment of concordant uranium-lead ages: Geochimica et Cosmochimica Acta, v. 62, p. 665-676.

Ludwig, K.R., 2002, SQUID 1.02, a user's manual: Berkeley Geochronology Center Special Publication 2, 17 p.

Ludwig, K.R., 2003, ISOPLOT/Ex version 3.0, a geochronological toolkit for Microsoft Excel: Berkeley Geochronology Center Special Publication 4, 71 p.

Mattinson, J.M., 2005, Zircon U-Pb chemical abrasion ("CA-TIMS") method: Combined annealing and multi-step partial dissolution analysis for improved precision and accuracy of zircon ages: Chemical Geology, v. 220, p. 47–66.

Parrish, R.R., Roddick, J.C., Loveridge, W.D., and Sullivan, R.D., 1987, Uranium-lead analytical techniques at the geochronology laboratory, Geological Survey of Canada, Radiogenic age and isotopic studies, Report 1: Geological Survey of Canada Paper 87-2, p. 3–7.

Pidgeon, R.T., Nemchin, A.A., and Hitchen, G.J., 1998, Internal structures of zircons from Archaean granites from the Darling Range Batholith; implications for zircon stability and the interpretation of zircon U-Pb ages: Contributions to Mineralogy and Petrology, v. 132, p. 288–299.

Premo, W.R., and Van Schmus, W.R., 1989, Zircon geochronology of Precambrian rocks in southeastern Wyoming and northern Colorado, *in* Grambling, J.A., and Tewksbury, B.J., eds., Proterozoic Geology of the Southern Rocky Mountains: Geological Society of America Special Paper 235, p. 13–32.

Rubatto, D., 2002, Zircon trace element geochemistry; partitioning with garnet and the link between U-Pb ages and metamorphism: Chemical Geology, v. 184, p. 123–138.

Schaltegger, U., Fanning, C.M., Gunther, D., Maurin, J.C., Schulmann, K., and Gebauer, D., 1999, Growth, annealing and recrystallization of zircon and preservation of monazite in high-grade metamorphism: conventional and in-situ U-Pb isotope, cathodoluminescence and microchemical evidence: Contributions to Mineralogy and Petrology, v. 134, p. 186–201.

Scoates, J.S., and Chamberlain, K.R., 1995, Baddeleyite (ZrO_2) and zircon ($ZrSiO_4$) from anorthositic rocks of the Laramie anorthosite complex, Wyoming; petrologic consequences and U-Pb ages: American Mineralogist, v. 80, p. 1317–1327.

Stacey, J.S., and Kramers, J.D., 1975, Approximation of terrestrial lead isotope evolution by a two-stage model: Earth and Planetary Science Letters, v. 36, p. 359–362.

Vavra, G., 1990, On the kinematics of zircon growth and its petrogenetic significance; a cathodoluminescence study: Contributions to Mineralogy and Petrology, v. 106, p. 90–99.

Vavra, G., 1994, Systematics of internal zircon morphology in major Variscan granitoid types: Contributions to Mineralogy and Petrology, v. 117, p. 331–344.

Vavra, G., Gebauer, D., Schmid, R., and Compston, W., 1996, Multiple zircon growth and recrystallization during polyphase Late Carboniferous to Triassic metamorphism in granulites of the Ivrea Zone (Southern Alps); an ion microprobe (SHRIMP) study: Contributions to Mineralogy and Petrology, v. 122, p. 337–358.

Watson, E.B., and Harrison, T.M., 1983, Zircon saturation revisited; temperature and composition effects in a variety of crustal magma types: Earth and Planetary Science Letters, v. 64, p. 295–304.

Williams, I.S., 1998, U-Th-Pb geochronology by ion microprobe, *in* McKibben, M.A., Shanks, W.C., and Ridley, W.I., eds., Applications of microanalytical techniques to understanding mineralization processes: Reviews in Economic Geology, v. 7, p. 1–35.

Woensdregt, C.F., 1992, Computation of surface energies in an electrostatic point charge model; 2, Application to zircon ($ZrSiO_4$): Physics and Chemistry of Minerals, v. 19, p. 59–69.

Appendix Figures

All ages are SHRIMP $^{207}Pb/^{206}Pb$ spot ages with 1σ errrors.

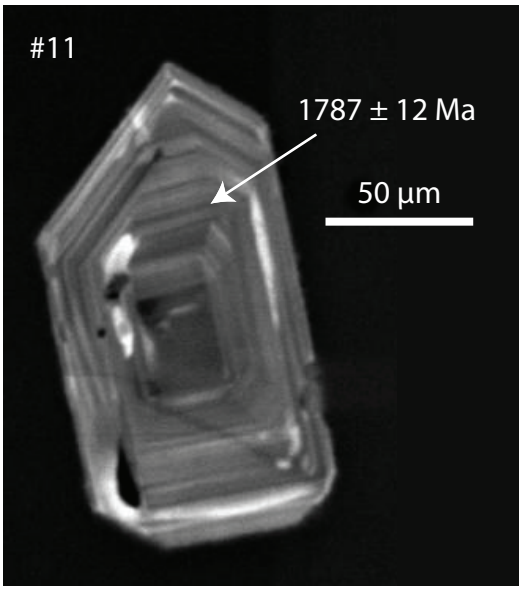

Figure A-1: Euhedral zircon from WRP 82-13. Crystal form and oscillatory zoning are consistent with igneous growth.

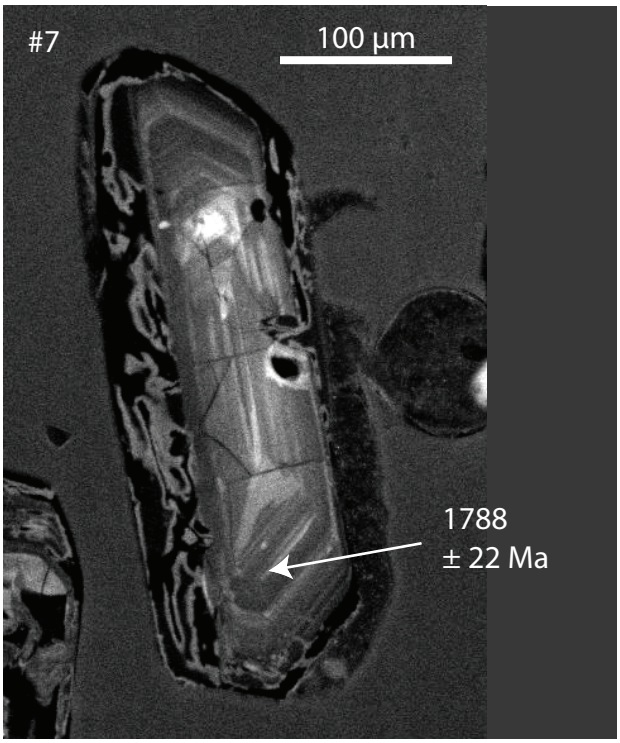

Figure A-2: Zircon from WRP 81-24 with an oscillatory zoned core overgrown by a younger, generally non-luminescent rim with stringy luminescent regions.

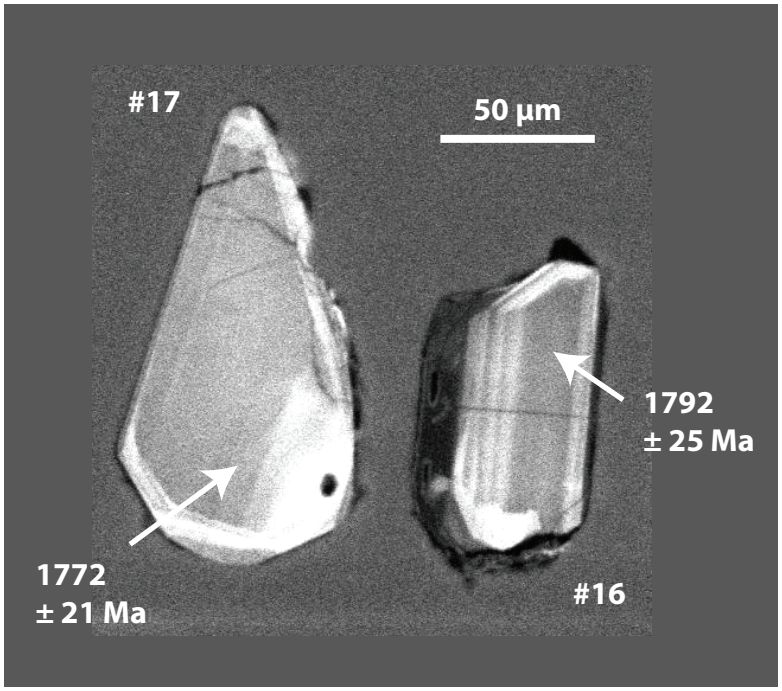

Figure A-3: Zircons from WRP 82-34. #17 shows faint oscillatory zonation and possible thin rims of non-luminescent material. #16 has an oscillatory-zoned core with a distinct younger rim of lower luminescent material similar to WRP 81-24 (Fig. A-2).

Appendix Figures

All ages are SHRIMP $^{207}Pb/^{206}Pb$ spot ages with 1σ errrors.

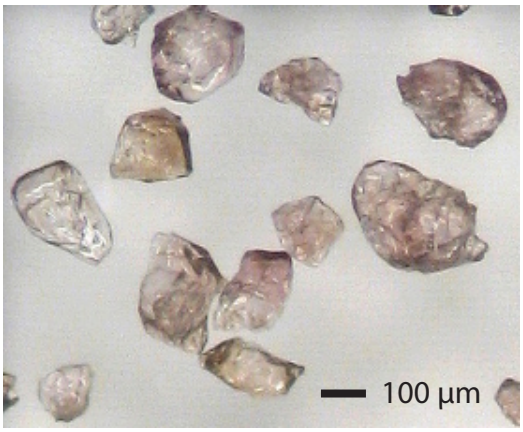

Figure A-4: Anhedral zircons from SM073r. Crystal form is consistent with igneous growth in a mafic rock.

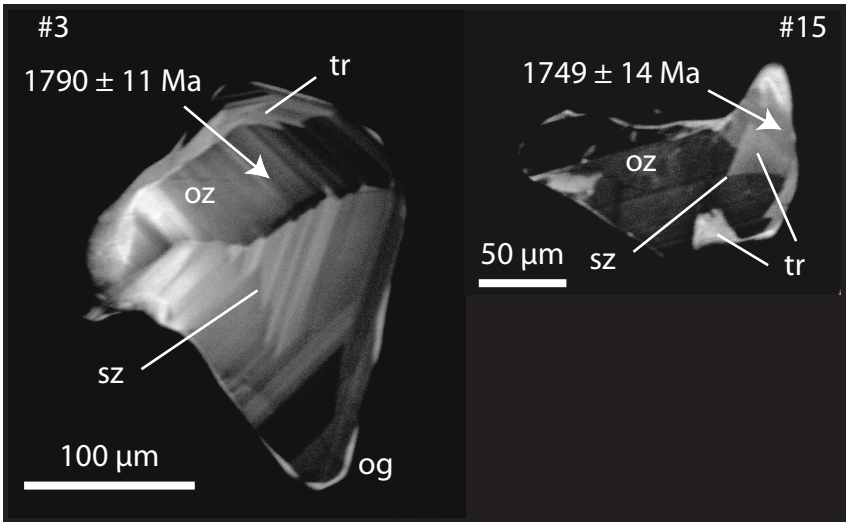

Figure A-5: CL images of SM073r zircons showing primary igneous oscillatory (oz) and sector zoning (sz). They are overprinted by transgressive recrystallization (tr) often bounded by original sector zones (#15), and thin overgrowths (og) representing one or two episodes of metamorphism.

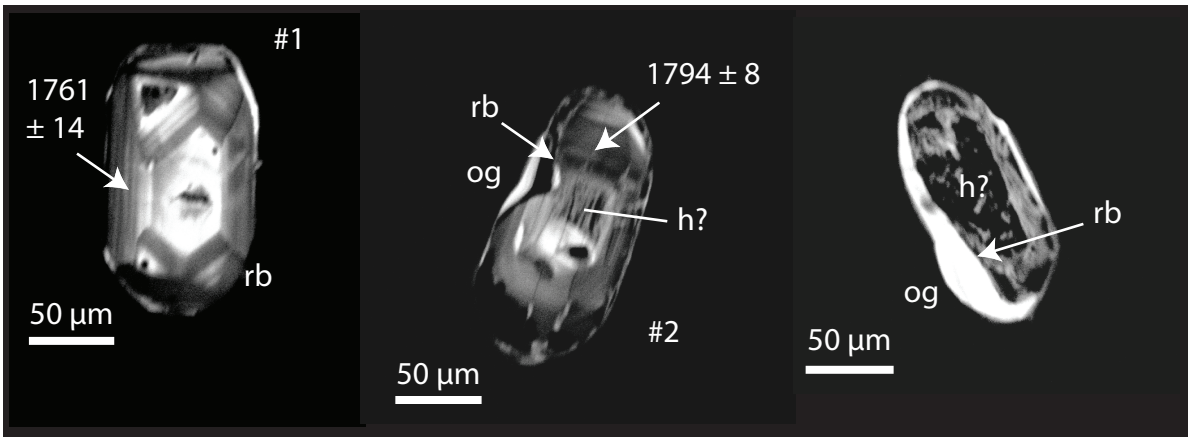

Figure A-6: CL images of SM357 zircons showing primary igneous oscillatory and sector zoning. Following initial growth, the zircons were partially resorbed (rb) and possibly hydrothermally altered (h?) prior to a final stage of strongly luminescent zircon overgrowth (og) interpreted as new metamorphic zircon.

Appendix Figures

All ages are SHRIMP $^{207}Pb/^{206}Pb$ spot ages with 1σ errrors.

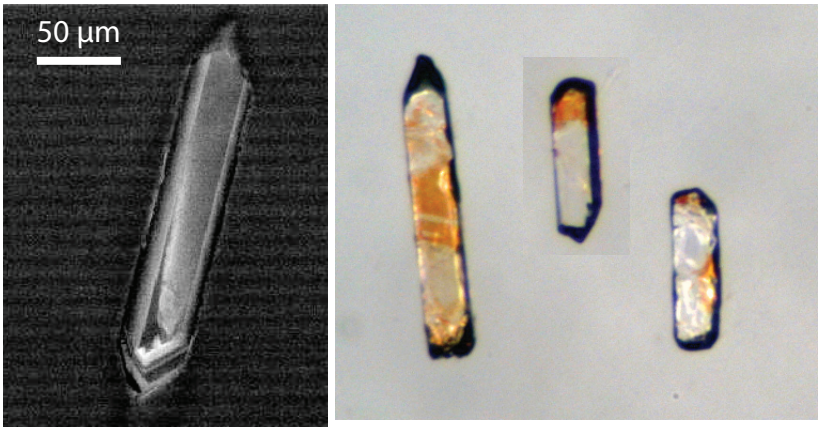

Figure A-7A: CL and transmitted light images of SM009 zircons. Igneous oscillatory zoning is visible along the margins of some grains. There is no visible evidence for overgrowths or resorption.

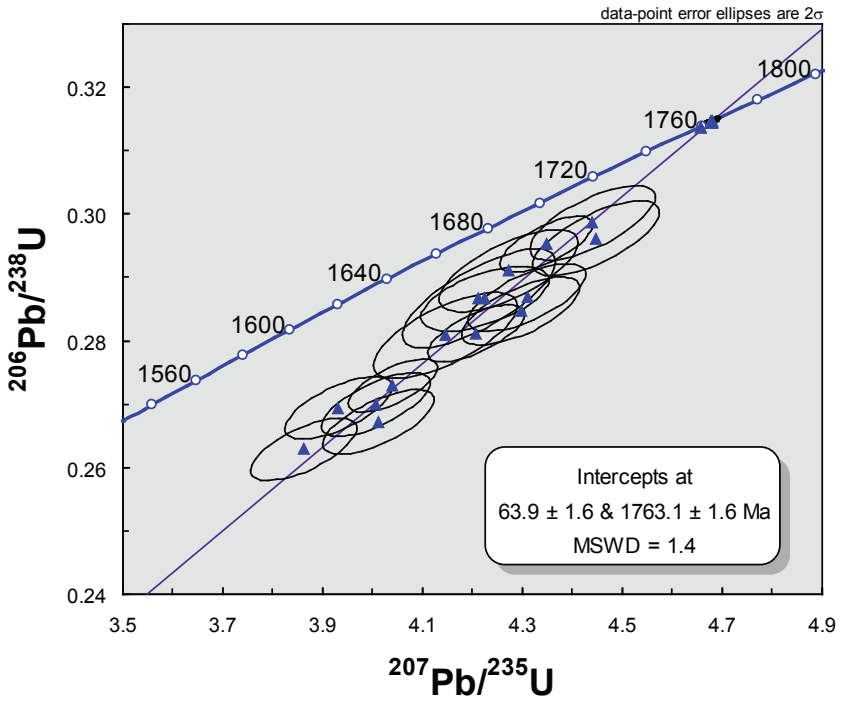

Figure A-7B: Composite concordia diagram showing the concordant CA-ID-TIMS results and the discordant SHRIMP results. Anchoring the discordia at the preferred crystallization age of 1763.1 ± 1.6 Ma results in a lower intercept age of ~64 Ma, consistent with Laramide uplift of the Sierra Madre

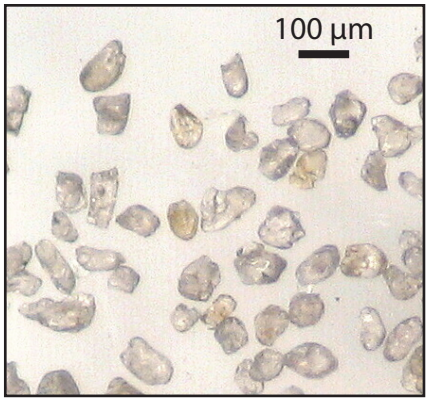

Figure A-8: Subhedral zircons from SM017r. Crystal form suggests that at least some grains grew freely in a melt.

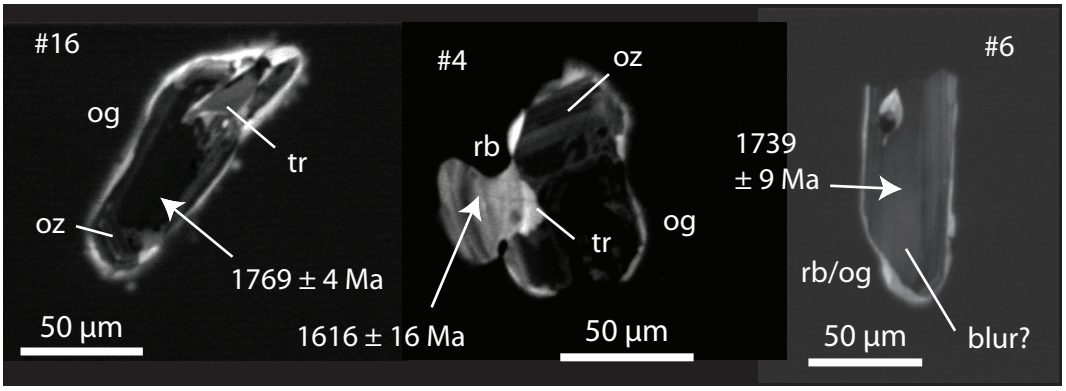

Figure A-9: CL images of SM017r zircons showing faint primary igneous oscillatory zoning (oz). They are overprinted by resorption (rb), transgressive recrystallization (tr), and thin, luminescent overgrowths (og) interpreted as metamorphic. Possible blurring and a small increase in CL intensity may reflect a ~1.745 metamorphic event.

Appendix Figures

All ages are SHRIMP $^{207}Pb/^{206}Pb$ spot ages with 1σ errrors.

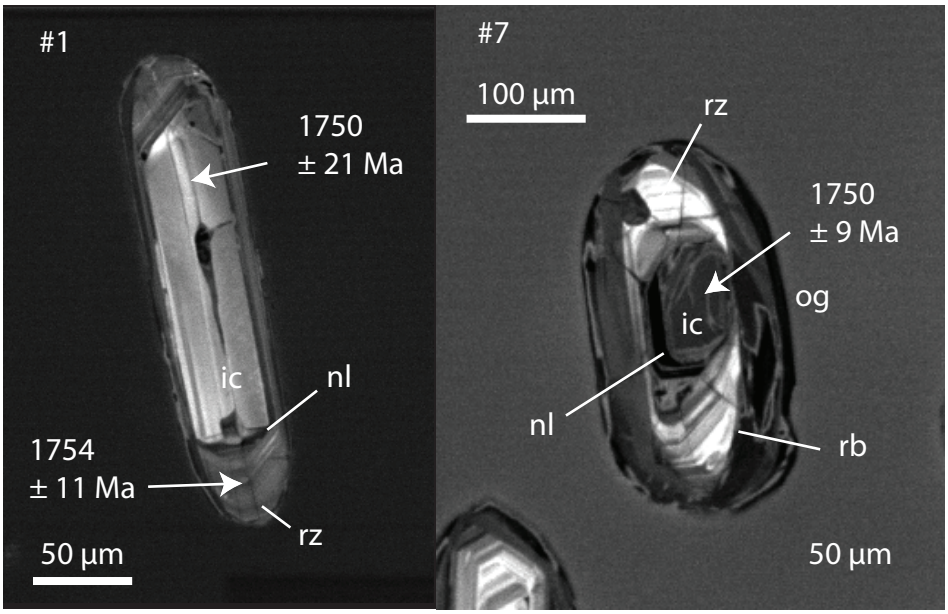

Figure A-10: CL images of SM045 zircons showing a primary igneous core (ic) with faint oscillatory zonation surrounded by a non-luminescent zone (nl) and a rim of modified zircon with relict oscillatory zoning (rz). These regions are overprinted by resorption (rb), which truncates original igneous zoning, followed by a non-luminescent, unzoned overgrowth (og). Grain #7 represents a fairly advanced stage of alteration and is not typical of the grains used to derive the age of the rock.

Figure A-11: BSE (a) and CL (b) images of a SM061r zircon showing faint, primary, igneous oscillatory zoning in both the inner core (ic) and outer core (oc) separated by a nonluminescent zone (nl). The core is overprinted by resorption (rb) which truncates original oscillatory zoning, and surrounded by irregular planar banded overgrowths (og) interpreted as metamorphic. Blurring of zonation in the inner and outer cores and production of the nonluminescent zone is interpreted as metemorphic recrystallization of unknown age. The nonluminescent band in the CL image is dark in the BSE image indicating that it is not composed of crystalline zircon. (The upper dark band in the BSE image is a fracture in the grain.)

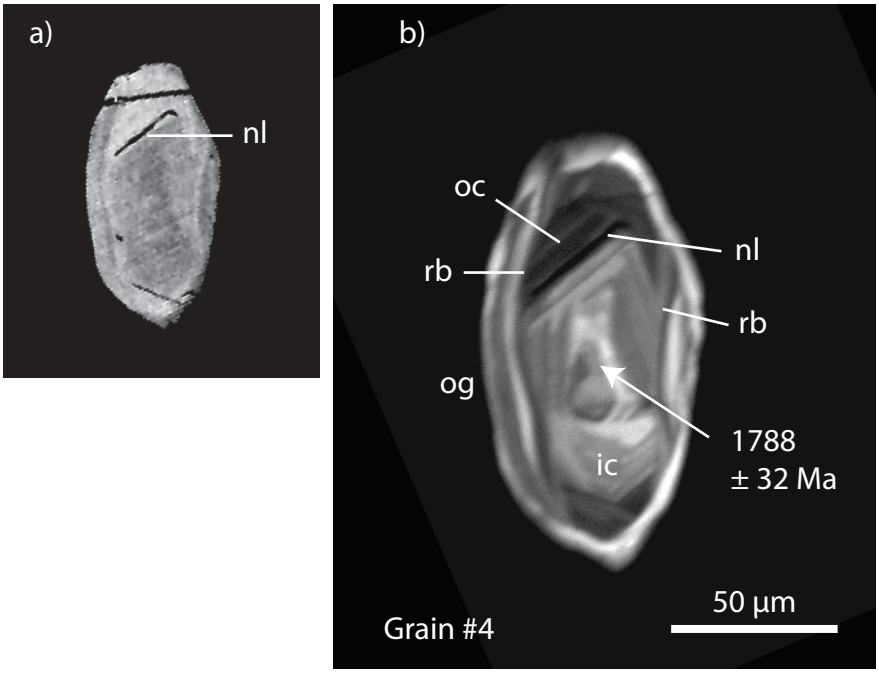

Appendix Figures

All ages are SHRIMP $^{207}Pb/^{206}Pb$ spot ages with 1σ errrors.

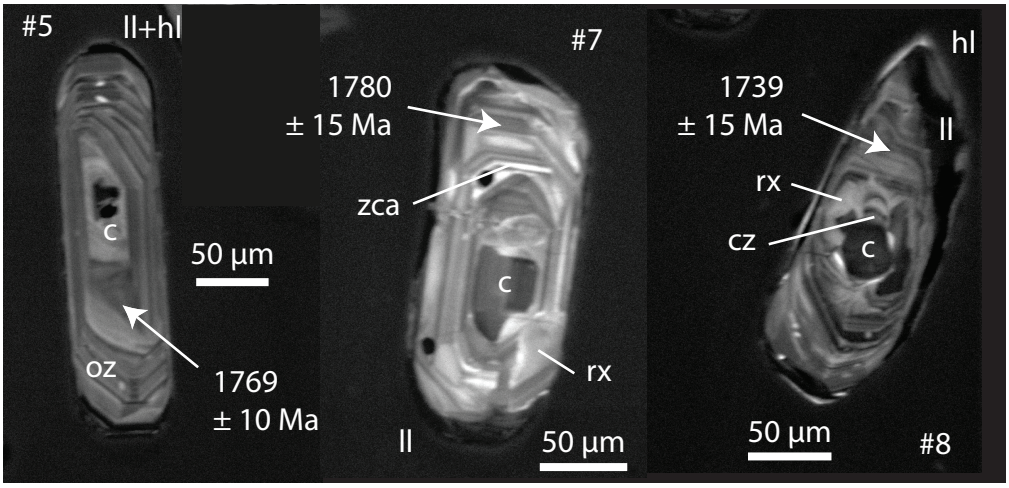

Figure A-12: CL images of SM290 zircons showing possible cores (c) that appear to be preferentially altered and possibly resorbed, overgrown by oscillatory zoned (oz) zircon modified by zone controlled alteration (zca; Vavra et al., 1996), convoluted zoning (cz), and recrystallization (rx). The progression from unaltered (#5) to predominantly zone altered (#7) to convoluted zoning (#8) may reflect a genetic sequence of increasing alteration. They are variably overprinted by resorption (rb), low-luminescence overgrowths (ll) and thin, outer, high luminescence overgrowths (hl) interpreted as metamorphic.

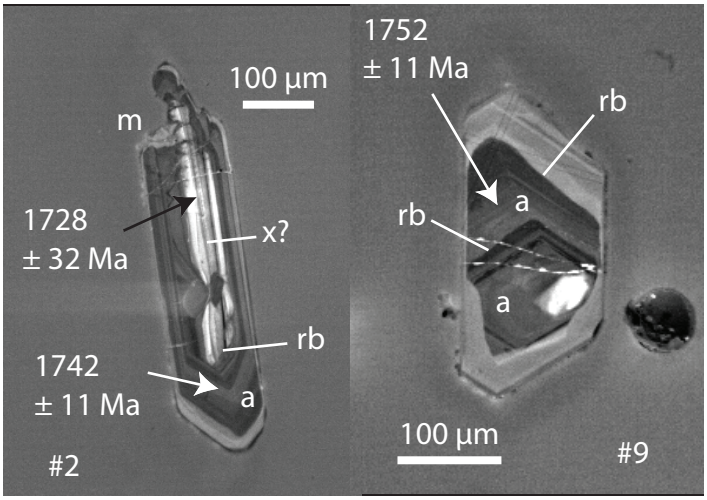

Figure A-13: CL images of SM058 zircons showing primary igneous oscillatory zoning in both the possibly xenocrystic cores (x?) and anatectic overgrowths (a). Resorption features (rb) are common both at the margin between cores and overgrowths (#2) as well as internal to the overgrowths (#9). Resorption surfaces within the overgrowths are interpreted as episodic zircon undersaturation during anatexis. Agreement between the spot ages of the xenocrystic core and anatectic overgrowth suggest that the age of the core was reset during anatexis. Late metamorphic recrystallization (m) is seen on #2. Polishing was not deep enough on #9 to expose any cores which may be present.

Table A-1. U-Th-Pb analytical data for SHRIMP spot analyses

Grains/ Spots	Interp	U (ppm)	Th (ppm)	Th/U	% comm ^{206}Pb	$^{206}Pb/^{238}U^{\#}$	± $^{206}Pb/^{238}U^{\S}$	$^{207}Pb/^{235}U^{\#}$	± $^{207}Pb/^{235}U^{\S}$	$^{207}Pb/^{206}Pb^{\#}$	± $^{207}Pb/^{206}Pb^{\S}$	$^{207}Pb/^{206}Pb$ Age Ma	± $^{207}Pb/^{206}Pb$ Age Ma §	% Discord†
WRP 82-13 (dacitic metavolcanic rock; igneous age 1781 +/- 8 Ma (MSWD 0.43); UTM NAD27 13 T 0341527; 4553772)														
1.1	ig	242	55	0.23	0.03	0.3101	0.7	4.62	1.0	0.1081	0.7	1768	13	2
2.1	ig	214	46	0.21	0.12	0.3137	0.8	4.68	1.2	0.1082	0.9	1770	16	1
3.1	ig	338	115	0.34	0.88	0.3034	0.6	4.58	1.3	0.1095	1.1	1791	21	5
4.1	ig	324	88	0.27	1.09	0.2964	0.7	4.61	1.5	0.1128	1.3	1846	24	10
5.1	ig	343	99	0.29	0.02	0.3028	0.6	4.57	0.9	0.1095	0.6	1792	12	5
6.1	ig	310	81	0.26	0.10	0.3116	0.7	4.68	1.1	0.1090	0.9	1783	16	2
6.2	ig	501	231	0.46	14.09	0.2292	1.0	3.82	7.0	0.1207	6.9	1967	123	48
7.1	ig	348	107	0.31	0.13	0.2931	0.7	4.40	1.0	0.1090	0.8	1782	14	8
8.1	ig	264	62	0.23	0.07	0.3013	0.7	4.49	1.1	0.1081	0.8	1768	15	4
9.1	ig	358	114	0.32	0.03	0.3072	0.6	4.60	0.9	0.1085	0.7	1775	12	3
10.1	ig	368	114	0.31	0.45	0.2968	0.6	4.42	1.2	0.1080	1.0	1766	19	5
11.1	ig	331	90	0.27	0.03	0.3122	0.6	4.70	0.9	0.1093	0.7	1787	12	2
12.1	ig	272	72	0.26	0.04	0.3050	0.7	4.57	1.0	0.1087	0.7	1778	13	4
SM073r (metagabbro; igneous age 1782 +/- 7 Ma (MSWD 0.92), minimum metamorphic age 1743 +/- 14 Ma (MSWD 0.52); UTM NAD27 13T 358479 4541169)														
1	ig	129	25	0.19	0.00	0.3061	0.9	4.59	1.3	0.1088	0.9	1780	17	3
2	ig	239	54	0.22	0.03	0.3103	0.7	4.62	1.0	0.1079	0.7	1765	13	1
3	ig	308	100	0.33	0.00	0.3146	0.6	4.75	0.9	0.1094	0.6	1790	11	2
4	bad	107	22	0.20	0.12	0.3212	1.1	4.73	1.6	0.1068	1.2	1745	21	-3
5	ig	272	72	0.26	0.05	0.3056	0.7	4.55	1.1	0.1080	0.8	1766	15	3
6	ig	529	120	0.23	0.01	0.3045	0.4	4.60	0.6	0.1096	0.5	1792	8	5
7	ig	441	143	0.32	0.00	0.3107	0.5	4.69	0.7	0.1096	0.5	1793	9	3
8	bad	240	64	0.27	0.37	0.3064	0.8	4.39	2.9	0.1038	2.8	1694	52	-2
9	ig	169	35	0.20	0.04	0.3169	0.8	4.73	1.2	0.1082	0.8	1769	15	0
10	ig	302	99	0.33	0.00	0.3102	0.6	4.65	0.9	0.1087	0.6	1778	11	2
11	ig	347	79	0.23	0.01	0.3142	0.6	4.70	0.8	0.1084	0.6	1773	10	1
12	ig	414	141	0.34	0.01	0.3142	0.5	4.73	0.7	0.1092	0.5	1787	9	1
13	rxtl	340	107	0.32	0.02	0.3058	0.6	4.48	0.8	0.1062	0.6	1735	11	1
14	rxtl	267	55	0.21	0.06	0.3135	0.7	4.63	1.0	0.1071	0.7	1751	13	0
15	rxtl	193	49	0.25	0.04	0.3104	0.8	4.58	1.1	0.1070	0.8	1749	14	0
SM357 (biotite granodiorite; igneous age 1777 +/- 11 Ma (MSWD 0.97); UTM NAD27 13 T 360740 4542708)														
1	ig	280	54	0.19	0.19	0.3188	0.6	4.74	1.0	0.1077	0.8	1761	14	-1
2	?	546	280	0.51	0.03	0.3054	0.4	4.62	0.6	0.1097	0.5	1794	8	4
3	ig	736	239	0.32	0.02	0.3111	0.4	4.63	0.6	0.1079	0.4	1765	8	1
4	ig	474	85	0.18	-0.02	0.3179	0.5	4.74	0.7	0.1082	0.5	1769	9	-1
5	ig	627	188	0.30	0.02	0.3196	0.4	4.77	0.6	0.1084	0.4	1772	8	-1
6	bad	306	103	0.34	0.86	0.2620	0.7	3.61	1.6	0.0999	1.4	1621	26	8
7	ig	395	105	0.27	0.03	0.3194	0.6	4.80	0.8	0.1091	0.6	1784	10	0
8	ig	296	101	0.34	0.03	0.3130	0.6	4.64	0.9	0.1075	0.7	1758	12	0

9	ig	464	317	0.68	0.16	0.3012	0.5	4.44	1.1	0.1070	1.0	1750	18	3
10	ig	279	63	0.23	0.00	0.3152	0.7	4.74	0.9	0.1090	0.6	1783	12	1
11	ig	540	246	0.45	0.03	0.3143	0.5	4.72	0.7	0.1090	0.5	1782	9	1
12	ig	378	142	0.38	0.15	0.3075	0.6	4.55	0.9	0.1072	0.7	1753	12	1
13	ig	534	164	0.31	0.05	0.3205	0.5	4.86	0.7	0.1099	0.5	1797	10	0
14	bad	245	252	1.03	0.91	0.3156	0.7	4.74	1.9	0.1091	1.8	1784	32	1

SM009 (garnet-bearing metagabbro; UTM NAD27 13 T 359189 4546742)

1	ig	158	51	0.32	0.02	0.2699	0.8	4.01	1.1	0.1076	0.8	1760	15	14
2	ig	168	58	0.35	0.04	0.2694	0.7	3.93	1.1	0.1059	0.8	1729	15	12
3	ig	228	78	0.34	0.00	0.2729	0.6	4.04	0.9	0.1074	0.7	1755	12	13
4	ig	166	56	0.34	0.17	0.2866	0.7	4.22	1.2	0.1069	1.0	1747	18	8
5	ig	90	24	0.26	0.00	0.2808	1.0	4.15	1.4	0.1071	1.0	1750	19	10
6	ig	95	31	0.33	0.00	0.2867	1.1	4.21	1.5	0.1066	1.0	1742	18	7
7	ig	250	115	0.46	0.01	0.2952	0.6	4.35	0.9	0.1068	0.6	1746	11	5
8	ig	151	50	0.33	0.04	0.2847	0.8	4.30	1.1	0.1095	0.8	1791	15	11
9	ig	104	36	0.35	0.00	0.2910	0.9	4.27	1.3	0.1064	1.0	1739	18	6
10	ig	209	76	0.36	0.02	0.2812	0.7	4.21	0.9	0.1085	0.7	1775	13	11
11	ig	128	44	0.34	0.00	0.2962	0.8	4.45	1.2	0.1089	0.8	1781	15	7
12	ig	154	54	0.35	0.02	0.2868	0.8	4.31	1.1	0.1090	0.8	1782	15	10
13	ig	136	51	0.37	0.00	0.2986	0.8	4.44	1.2	0.1078	0.8	1763	15	5
14	ig	161	55	0.34	0.03	0.2629	0.8	3.86	1.1	0.1066	0.8	1741	15	16
15	ig	148	50	0.34	0.00	0.2672	0.8	4.01	1.1	0.1089	0.8	1781	15	17

SM017r (garnet-bearing metagabbro; igneous age ~1763 Ma; UTM NAD27 13 T 359189 4546742)

1	ig	873	510	0.58	0.00	0.2760	0.3	4.12	0.5	0.1084	0.3	1773	6	13
2	ig	937	534	0.57	0.03	0.2472	0.4	3.60	0.5	0.1058	0.4	1727	6	21
3	mix?	1209	1363	1.13	0.00	0.2825	0.3	4.18	0.4	0.1074	0.3	1755	5	9
4	rim	201	57	0.28	0.08	0.2570	0.7	3.53	1.1	0.0995	0.9	1616	16	10
5	bad	121	25	0.21	4.36	0.2700	0.9	3.59	3.6	0.0965	3.5	1558	66	1
6	ig	483	298	0.62	0.02	0.2762	0.4	4.05	0.6	0.1064	0.5	1739	9	11
7	rxtl?	96	24	0.25	0.44	0.2598	1.0	3.71	1.9	0.1035	1.7	1688	31	13
8	bad	2052	3157	1.54	0.01	0.1241	0.3	1.63	0.4	0.0950	0.3	1528	6	103
9	bad	105	23	0.22	2.94	0.2780	1.0	3.86	5.1	0.1006	5.0	1635	92	3
10	ig	548	411	0.75	0.89	0.2887	0.4	4.29	0.9	0.1077	0.8	1761	15	8
11	ig	776	606	0.78	0.00	0.2862	0.3	4.21	0.5	0.1068	0.4	1745	7	8
12	ig	722	430	0.60	0.01	0.2873	0.4	4.15	0.5	0.1047	0.4	1708	7	5
13	rim?	95	20	0.21	0.20	0.2807	1.0	3.79	1.6	0.0980	1.3	1587	24	-1
14	rxtl?	97	22	0.23	0.09	0.2918	1.0	4.23	1.4	0.1051	1.1	1715	20	4
15	ig	1028	846	0.82	0.00	0.2971	0.3	4.41	0.4	0.1077	0.3	1761	6	5
16	ig	1822	1242	0.68	0.01	0.2863	0.2	4.27	0.3	0.1082	0.2	1769	4	9
17	mix	175	110	0.63	0.06	0.2760	0.7	3.90	1.0	0.1024	0.8	1669	14	6
18	rim	137	34	0.25	0.15	0.2739	0.9	3.79	1.4	0.1003	1.1	1630	20	4
19	ig	871	715	0.82	0.00	0.2720	0.3	4.09	0.5	0.1089	0.3	1782	6	15
20	ig	315	224	0.71	-0.03	0.2641	0.5	3.89	0.8	0.1067	0.6	1745	10	15

WRP 81-24 (Sierra Madre Granite; igneous age 1763 +/- 9 Ma (MSWD 0.53); UTM NAD27 13 T 343576 4544129)

1	ig	73	18	0.24	0.15	0.3092	1.42	4.59	1.85	0.1076	1.2	1759	22	1
2	ig	580	102	0.18	0.21	0.3068	1.04	4.56	1.15	0.1077	0.5	1762	9	2
3	ig	113	34	0.30	0.24	0.3091	1.28	4.60	1.68	0.1080	1.1	1767	20	2
4	ig	394	71	0.18	8.84	0.2381	1.12	3.51	3.22	0.1071	3.0	1749	55	27
5	ig	256	22	0.09	0.96	0.1921	1.15	2.85	1.79	0.1077	1.4	1761	25	55
6	ig	117	35	0.30	0.31	0.3092	1.31	4.59	2.02	0.1077	1.5	1760	28	1
7	ig	338	57	0.17	1.04	0.2182	1.09	3.29	1.64	0.1094	1.2	1788	22	41
8	ig	610	83	0.14	0.69	0.2905	1.05	4.28	1.48	0.1070	1.0	1748	19	6
9	ig	140	38	0.27	0.32	0.2851	1.25	4.20	1.69	0.1070	1.1	1749	21	8
10	ig	256	54	0.21	3.33	0.3040	1.19	4.53	3.54	0.1082	3.3	1769	61	3
11	ig	115	27	0.23	0.39	0.2885	1.28	4.29	1.82	0.1079	1.3	1764	24	8
12	bad	746	174	0.23	22.21	0.1473	1.73	2.10	14.33	0.1036	14.2	1688	262	91
13	ig	164	43	0.26	0.20	0.3022	1.26	4.44	1.69	0.1065	1.1	1740	20	2
14	ig	102	22	0.22	0.08	0.3199	1.32	4.68	1.85	0.1061	1.3	1733	24	-3
15	ig	428	69	0.16	0.65	0.2591	1.07	3.88	1.60	0.1085	1.2	1775	22	20
16	ig	445	83	0.19	0.16	0.3018	1.06	4.47	1.26	0.1075	0.7	1758	12	3
17	ig	133	36	0.27	0.42	0.2723	1.34	4.13	1.85	0.1100	1.3	1800	23	16
18	ig	182	39	0.22	0.88	0.2988	1.23	4.42	2.26	0.1074	1.9	1756	35	4
19	ig	368	72	0.19	0.65	0.3020	1.09	4.53	1.62	0.1089	1.2	1781	22	5
20	ig	273	55	0.20	0.04	0.3188	1.12	4.76	1.28	0.1082	0.6	1770	11	-1

WRP 82-34 (Sierra Madre Granite; igneous age 1766 +/- 8 Ma (MSWD 1.3); UTM NAD27 13 T 338617 4544885)

1	ig	155	39	0.25	0.11	0.3087	1.15	4.62	1.38	0.1086	0.8	1775	14	2
2	ig	171	51	0.30	0.06	0.3069	1.14	4.62	1.38	0.1093	0.8	1787	14	4
3	ig	170	57	0.34	0.01	0.2809	1.23	4.23	1.45	0.1092	0.8	1787	14	12
4	ig	373	82	0.22	0.21	0.3017	1.04	4.44	1.20	0.1069	0.6	1747	11	3
5	ig	107	26	0.24	0.14	0.3199	1.27	4.65	1.65	0.1054	1.1	1721	19	-4
6	ig	70	19	0.28	0.17	0.3061	1.47	4.50	2.02	0.1066	1.4	1742	26	1
7	bad	90	10	0.12	1.02	0.0718	1.54	1.03	3.50	0.1043	3.1	1701	58	281
8	bad	307	74	0.24	1.97	0.1872	1.26	2.52	5.06	0.0977	4.9	1582	92	43
9	ig	119	38	0.32	0.00	0.3117	1.29	4.65	1.61	0.1083	1.0	1771	18	1
10	bad	252	50	0.20	1.80	0.1958	1.15	2.86	2.40	0.1060	2.1	1732	39	50
11	ig	82	17	0.21	0.00	0.3026	1.43	4.51	1.85	0.1080	1.2	1766	22	4
12	ig	94	22	0.24	0.08	0.3112	1.34	4.61	1.77	0.1073	1.2	1755	21	0
13	ig	231	51	0.22	-0.03	0.3090	1.11	4.62	1.28	0.1085	0.6	1774	12	2
14	ig	184	49	0.27	0.09	0.3085	1.15	4.57	1.39	0.1075	0.8	1758	14	1
15	ig	165	38	0.23	0.12	0.3120	1.17	4.68	1.44	0.1089	0.8	1781	15	2
16	ig	74	22	0.29	0.20	0.3056	1.45	4.62	2.00	0.1096	1.4	1792	25	4
17	ig	96	28	0.29	0.11	0.2967	1.36	4.43	1.78	0.1084	1.1	1772	21	6

SM045 (Migmatitic augen gneiss; igneous age 1769 +/- 10 Ma (MSWD 0.61); metamorphic ages 1752 +/- 13, 1618 +/- 9 Ma; UTM NAD27 13 T 351034 4545207)

1.1	ig	143	47	0.33	0.25	0.2929	0.8	4.32	1.4	0.1071	1.2	1750	21	6
1.2	ig	329	69	0.21	0.05	0.2981	0.6	4.41	0.8	0.1073	0.6	1754	11	4
2	ig	384	128	0.33	0.02	0.3193	1.5	4.74	1.6	0.1077	0.6	1761	11	-1
3	ig	141	44	0.31	0.00	0.3101	0.8	4.59	1.2	0.1074	0.8	1757	15	1

4	ig	209	101	0.48	0.02	0.3347	0.7	5.01	1.0	0.1086	0.7	1776	13	-5
5	ig	488	177	0.36	0.01	0.3216	1.2	4.84	1.4	0.1091	0.7	1785	12	-1
6	ig	171	49	0.29	0.27	0.3103	0.8	4.69	1.3	0.1096	1.0	1793	19	3
7.1	ig	712	216	0.30	0.14	0.2628	0.4	3.88	0.7	0.1071	0.5	1750	9	16
7.2	bad	856	7	0.01	2.66	0.2664	0.4	3.71	2.6	0.1010	2.6	1642	48	8
8	ig	165	49	0.30	0.35	0.3208	0.8	4.77	1.4	0.1078	1.1	1762	20	-2
9	ig	171	58	0.34	0.08	0.3146	0.8	4.70	1.1	0.1084	0.9	1773	16	1
10	rim	548	1	0.00	0.08	0.2916	0.4	4.00	0.7	0.0994	0.5	1613	10	-2
11	ig	137	45	0.33	0.06	0.3030	0.8	4.51	1.2	0.1080	0.9	1766	17	4
12	rim	995	4	0.00	0.07	0.2911	0.3	3.98	0.5	0.0992	0.4	1609	8	-2
13	mix?	698	2	0.00	0.14	0.3233	0.4	4.56	0.6	0.1022	0.5	1664	9	-8
14	mix?	543	1	0.00	0.03	0.3054	0.4	4.25	0.6	0.1010	0.5	1643	9	-4
15	mix?	616	4	0.01	0.29	0.3139	0.4	4.53	0.7	0.1046	0.6	1708	11	-3
16	mix?	556	1	0.00	0.06	0.2992	0.5	4.23	0.7	0.1026	0.6	1672	11	-1
17	bad	520	1	0.00	2.59	0.3134	0.5	4.42	2.0	0.1022	1.9	1664	36	-5
18	rim	1102	4	0.00	0.02	0.2885	0.3	3.98	0.4	0.1001	0.3	1625	6	-1

SM061r (Augen gneiss; igneous age 1759 +/- 8 Ma (MSWD 1.03); metamorphic age ~1.6 Ga; UTM NAD27 13 T 356260 4548375)

1	bad	39	6	0.14	0.79	0.3204	2.0	4.36	4.2	0.0986	3.7	1599	69	-11
2	ig	140	40	0.29	0.15	0.3117	0.9	4.59	1.4	0.1067	1.0	1744	19	0
3	rim	136	12	0.09	0.20	0.2930	0.9	3.99	1.7	0.0988	1.4	1601	26	-3
4	ig	99	25	0.25	0.00	0.3152	1.1	4.75	2.0	0.1093	1.8	1788	32	1
5.1	rxtl?	277	44	0.16	0.06	0.3079	0.6	4.50	0.9	0.1061	0.7	1733	13	0
5.2	bad	57	5	0.08	0.54	0.2938	1.4	3.81	2.8	0.0939	2.5	1507	47	-9
6	ig	105	23	0.22	-0.18	0.3145	1.1	4.76	1.7	0.1097	1.3	1795	23	2
7	ig	171	41	0.24	0.12	0.3135	0.8	4.59	1.4	0.1061	1.2	1734	21	-1
8.1	mix?	179	27	0.15	0.01	0.2761	0.8	3.84	1.2	0.1009	0.9	1641	17	4
8.2	ig	341	51	0.15	0.06	0.3039	0.6	4.47	0.9	0.1067	0.7	1744	12	2
9.1	ig	229	59	0.26	0.00	0.3207	0.7	4.76	1.0	0.1077	0.7	1761	13	-2
9.2	ig	196	38	0.19	0.02	0.3350	0.7	5.04	1.0	0.1092	0.7	1785	13	-4
10	rxtl?	123	23	0.18	0.28	0.2795	1.0	3.89	1.8	0.1009	1.5	1641	28	3
11	ig	195	35	0.18	-0.07	0.3133	0.8	4.63	1.1	0.1071	0.8	1751	15	0
12	rxtl?	313	12	0.04	0.05	0.3005	0.6	4.28	0.9	0.1034	0.7	1685	13	0
13.1	ig	141	27	0.19	0.00	0.3213	0.9	4.79	1.2	0.1081	0.9	1768	16	-2
13.2	ig	89	17	0.19	0.08	0.3235	1.2	4.73	1.8	0.1060	1.3	1731	24	-4
14	ig	110	26	0.24	0.11	0.3115	1.1	4.66	1.7	0.1085	1.3	1774	24	2
15.1	rxtl?	367	36	0.10	-0.04	0.3095	0.6	4.54	0.9	0.1063	0.7	1737	14	0
15.2	ig	356	119	0.33	0.02	0.3199	0.6	4.72	0.8	0.1069	0.6	1748	11	-2
16.1	rim	99	10	0.10	0.00	0.3100	1.3	4.20	2.0	0.0982	1.4	1590	27	-9
16.2	ig	286	80	0.28	-0.05	0.3507	0.7	5.20	1.9	0.1076	1.8	1759	32	-9
17	ig	155	47	0.30	0.37	0.3202	1.0	4.76	2.2	0.1077	1.9	1762	35	-2
18	ig	243	45	0.18	0.09	0.3068	0.8	4.57	1.2	0.1081	0.9	1767	16	2
19	rxtl?	193	12	0.06	0.02	0.3048	0.8	4.38	1.3	0.1041	1.0	1699	19	-1
20	rxtl?	165	13	0.08	0.19	0.2977	0.8	4.18	1.3	0.1017	1.1	1656	20	-1
21	ig	107	22	0.21	0.06	0.3078	1.0	4.61	1.5	0.1086	1.0	1777	19	3
22	rxtl?	231	18	0.08	0.08	0.3311	0.8	4.71	1.1	0.1032	0.9	1683	16	-9

SM290 (Augen gneiss; igneous age 1766 +/- 10 Ma (MSWD 0.56); metamorphic age 1611 +/- 22 Ma; UTM NAD27 13 T 374272 4540705)

1	ig	484	104	0.22	0.06	0.3078	0.5	4.57	0.7	0.1078	0.5	1762	9	2
2.1	ig	255	40	0.16	-0.04	0.3144	0.7	4.69	1.1	0.1081	0.9	1768	16	0
2.2	met	864	1	0.00	0.00	0.2992	0.4	4.19	0.6	0.1015	0.4	1651	8	-2
3	ig	334	115	0.34	0.07	0.2973	0.6	4.42	0.9	0.1077	0.6	1761	12	5
4	rim?	376	3	0.01	0.03	0.2813	0.5	3.85	0.8	0.0993	0.6	1611	11	1
5	ig	356	56	0.16	0.02	0.3110	0.6	4.64	0.8	0.1082	0.6	1769	10	1
6	ig	296	51	0.17	0.02	0.3102	0.6	4.64	0.9	0.1084	0.6	1773	11	2
7	ig	180	42	0.23	0.05	0.3119	0.8	4.68	1.1	0.1089	0.8	1780	15	2
8	rxtl	284	40	0.14	0.34	0.3034	0.6	4.45	1.0	0.1064	0.8	1739	15	2
9	ig	175	26	0.15	0.55	0.3015	0.7	4.51	1.4	0.1086	1.2	1776	21	5
10	ig	197	25	0.13	0.12	0.3056	0.8	4.60	1.2	0.1091	0.9	1784	16	4
11	ig	496	86	0.17	0.00	0.3105	0.5	4.62	0.7	0.1078	0.5	1763	9	1
12	ig	496	88	0.18	0.02	0.3075	0.5	4.55	0.7	0.1074	0.5	1755	9	2
13	ig	607	152	0.25	0.05	0.3166	0.4	4.71	0.6	0.1078	0.4	1763	8	-1

SM058 (Metawacke leucosome; anatectic age 1747 +/- 7 Ma (MSWD 0.63); UTM NAD27 13 T 354974 4548522)

1.1	ig	85	27	0.31	0.18	0.2838	1.1	4.18	2.1	0.1068	1.8	1745	32	8
1.2	ig	297	56	0.19	0.05	0.3097	0.6	4.62	0.8	0.1081	0.6	1767	11	2
2.1	ig	171	112	0.66	0.94	0.2944	0.8	4.29	1.9	0.1058	1.8	1728	32	4
2.2	ig	297	27	0.09	0.05	0.3112	0.6	4.57	0.8	0.1066	0.6	1742	11	0
3	ig	261	40	0.15	0.05	0.3119	0.6	4.62	1.0	0.1074	0.8	1756	14	0
4	ig	344	45	0.13	0.02	0.3143	0.5	4.63	0.8	0.1068	0.5	1746	10	-1
5	rxtl?	335	36	0.11	0.08	0.3047	0.5	4.41	0.8	0.1049	0.6	1713	11	0
6	ig	247	45	0.18	0.49	0.3008	0.7	4.41	1.2	0.1064	1.0	1739	18	3
7	ig	319	42	0.13	0.07	0.3055	0.5	4.47	0.8	0.1062	0.6	1734	11	1
8	ig	338	98	0.29	0.89	0.2853	0.5	4.19	1.7	0.1065	1.7	1741	31	8
9	ig	276	45	0.16	0.01	0.3067	0.6	4.53	0.8	0.1072	0.6	1752	11	2
10.1	bad	130	25	0.19	2.71	0.2958	1.0	4.24	5.5	0.1039	5.4	1694	100	1
10.2	ig	383	73	0.19	0.01	0.3126	0.5	4.60	0.7	0.1066	0.5	1743	9	-1
11	ig	79	43	0.54	0.20	0.2917	1.1	4.33	1.7	0.1077	1.3	1760	24	7
12	rim	167	11	0.06	0.09	0.2905	0.7	4.05	1.1	0.1012	0.9	1646	16	0
13	ig	96	32	0.33	0.10	0.2781	1.0	4.15	1.5	0.1082	1.2	1770	21	12
14	ig	195	93	0.48	0.05	0.3076	0.7	4.50	1.0	0.1062	0.7	1735	13	0
15	ig	177	416	2.35	2.21	0.2534	0.8	3.68	2.4	0.1053	2.3	1719	43	18

Notes:

* common Pb.

[#] atomic ratios corrected for initial Pb using amount of 204Pb and corresponding average Earth values from Stacey and Kramers (1975)

[§] errors given at 1 sigma level

[†] degree of discordance, percentage of distance that analysis lies along a chord from its extrapolated intersection with concordia (corresponding to its $^{207}Pb/^{206}Pb$ age) to the origin at 0 Ma.

Interpretation: ig = igneous crystallization age; rim = metamorphic rim; rxtl = metamorphic recrystallization; bad = bad data point (high errors or common Pb); mix = multiple age domains

Table A-2: U-Pb CA-ID-TIMS zircon data

SM009 Fe-rich orthoamphibolite (UTM NAD27 13 T 356653 4545464)
1764.2±1.4 (MSWD = 1.5) 4 point* weighted 207Pb/206Pb date, Concordia Age = 1763.1 ±1.6 Ma (MSWD = 0.14)

								Corrected atomic ratios												
	Weight	U	sample Pb		initial Pb		Pb*	206Pb	208Pb	206Pb/238U		207Pb/235U		207Pb/206Pb		206/238	207/235	207/206			
Sample	(µg)	(ppm)	(ppm)	(pg)	(ppm)	(pg)	Pbc	204Pb	206Pb	(rad.)	%err	(rad.)	%err	(rad.)	%err	Age (Ma)	Age (Ma)	Age (Ma)	err	Rho	% disc.
sA aa*	8.48	69.5	23.0	195	0.35	2.9	29.9	3682	0.10	0.3144	(0.09)	4.6790	(0.12)	0.1079	(0.08)	1762.3	1763.5	1765.0	±1.5	0.73	0.18
sB aa*	8.07	60.3	19.7	159	0.00	0.0	75.0	2.2E+06	0.10	0.3143	(0.07)	4.6771	(0.09)	0.1079	(0.06)	1762.1	1763.2	1764.4	±1.1	0.76	0.16
sC aa*	7.34	33.8	11.1	81	0.00	0.0	26.3	2.8E+06	0.10	0.3146	(0.06)	4.6760	(0.14)	0.1078	(0.11)	1763.3	1762.9	1762.5	±1.9	0.68	-0.05
sE	9.15	102.8	33.8	309	0.17	1.6	60.9	11039	0.10	0.3135	(0.06)	4.6557	(0.08)	0.1077	(0.05)	1758.1	1759.3	1760.7	±1.0	0.77	0.17
sG*	3.41	143.9	47.4	162	0.11	0.4	41.7	523	0.11	0.3146	(0.09)	4.6796	(0.13)	0.1079	(0.09)	1763.4	1763.6	1763.8	±1.6	0.74	0.02

Notes: sample: s_=single grain, aa=mechanically air abraded, *used in age calculations
Weight: represents estimated weight prior to first step of CATIMS dissolution. U and Pb concentrations are based on this weight and the U and Pb atoms measured from the second dissolution step only. The U and Pb concentrations may be underestimations, depending on how much material was dissolved and leached in the first step. They are useful for internal comparisons however. Picograms (pg) sample and initial Pb from the second dissolution step are measured directly.
sample Pb: sample Pb (radiogenic + initial) corrected for laboratory blank
initial Pb: common Pb corrected for laboratory blank of 3.5 pg Pb for zircon analyses.
Pb*/Pbc: radiogenic Pb to total common Pb (blank + initial)
Corrected atomic ratios: $^{206}Pb/^{204}Pb$ corrected for blank, mass discrimination and tracer, all others corrected for blank, mass discrimination, tracer and initial Pb, values in parentheses are 2 sigma errors in percent.
Rho: $^{206}Pb/^{238}U$ vs $^{207}Pb/^{235}U$ error correlation coefficient
% disc.: percent discordant

Zircon dissolution and chemistry were adapted from methods developed by Krogh (1973), Parrish et al. (1987) and Mattinson (2005). All zircons were chemically abraded (CATIMS). Final dissolutions were spiked with a mixed $^{205}Pb/^{233}U/^{235}U$ tracer (ET535). Pb and U samples were loaded onto single rhenium filaments with silica gel and graphite, respectively; isotopic compositions were measured in multi-collector, static mode on a Micromass Sector 54 thermal ionization mass spectrometer at the University of Wyoming with ^{204}Pb in Daly-photomultiplier collector and all other isotopes in Faraday collectors. Mass discrimination of 0.059 ± 0.05 %/amu for Pb was determined by replicate analyses of NIST SRM 981. U fractionation was determined internally during each run. Procedural blanks averaged 3.5 pg Pb during the course of the study. Isotopic composition of the Pb blank was estimated as 19.09±0.5, 15.652±0.2, and 38.81±.2 for 206/204, 207/204 and 208/204, respectively. U blanks were consistently less than 0.6 pg. Concordia coordinates, intercepts, and uncertainties were calculated using MacPBDAT and ISOPLOT programs (based on Ludwig 1988, 1991); initial Pb isotopic compositions were estimated by Stacey and Kramers (1975) model. The decay constants used by MacPBDAT are those recommended by the I.U.G.S. Subcommission on Geochronology (Steiger and Jäger, 1977): 0.155125 x 10^{-9}/yr for ^{238}U, 0.98485 x 10^{-9}/yr for ^{235}U and present-day $^{238}U/^{235}U$ = 137.88.